

Quasi-Particle Dynamics in Superconducting Aluminum

Katrin Steinberg, Marc Scheffler, and Martin Dressel

1. *Physikalisches Institut, Universität Stuttgart, Pfaffenwaldring 57, D-70550 Stuttgart, Germany*

(Dated: Received November 26, 2024)

The response of superconducting aluminum to electromagnetic radiation is investigated in a broad frequency (45 MHz to 40 GHz) and temperature range ($T > T_c/2$), by measuring the complex conductivity. While the imaginary part probes the superfluid density (Cooper-pairs), the real part monitors the opening of the superconducting energy gap and – most important here – the zero-frequency quasi-particle response. Here we observe the full temperature and frequency dependence of the coherence peak. Varying the mean free path gives insight into the dynamics, scattering and coherence effects of the quasi-particles in the superconducting state.

PACS numbers: 74.25.Gz, 74.25.Nf, 74.70.Ad, 74.78.Db

I. INTRODUCTION

Microwave and optical experiments have played a prominent role in the elucidation of the superconducting state for more than fifty years, because they provide information on the single-particle excitations as well as on the response of the Cooper pairs.^{1,2} The electrodynamic properties of superconductors can be calculated on the basis of the BCS theory,³ as first worked out by Mattis and Bardeen;⁴ and there exist precise predictions on the temperature and frequency dependence of the complex conductivity. One of the hallmarks of the superconducting state is the opening of an energy gap Δ in the density of states right below the critical temperature T_c ; both are related by mean-field theory: $2\Delta = 3.53k_B T_c$. In the 50s and 60s of the last century, enormous efforts were undertaken to explore the microwave and THz absorption of superconductors, like Al, In, or Sn, in order to obtain the conductivity in the region of the superconducting gap.⁵ Much less is known about the response of the quasi-particles in the superconducting state where, at energies below the energy gap, a maximum in the electromagnetic absorption – the so-called coherence peak – is expected for temperatures slightly below the superconducting transition (Fig. 1). The analog feature in nuclear magnetic resonance, i.e. the presence of a maximum in the nuclear-spin relaxation-rate of aluminum below T_c ,⁷ was one of the crucial experiments for the quick success of the BCS theory. By now, this Hebel-Slichter peak has been found in a large number of superconductors. In the case of the electrodynamic response, the experimental confirmation of the coherence peak turned out to be much more difficult⁸ and it was only in the 1990s, that a maximum in the temperature dependent conductivity was observed by studying Pb and Nb in a microwave cavity at 60 GHz.^{9,10} The complete mapping of the conductivity coherence peak, in particular its frequency dependence, has not been performed experimentally, even fifty years after the BCS theory.

During recent years the issue of the quasi-particle dynamics has attracted considerable interest in the field of high-temperature superconductors.¹¹ While a general agreement exists that no well-defined superconduct-

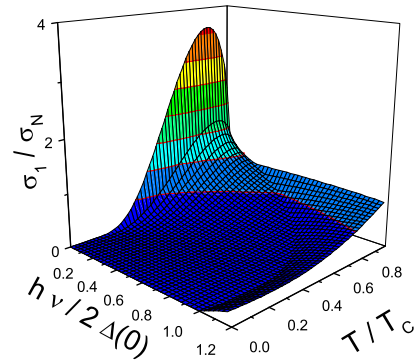


FIG. 1: (color online) Frequency and temperature dependence of the real part of the conductivity σ_1/σ_n calculated according the BCS theory^{4,6} with the ratio of the coherence length to the mean free path $\pi\xi(0)/2\ell = 10$. The pronounced maximum for low frequencies at a temperature slightly below T_c is the coherence peak.

ing gap opens, there remain questions of the residual absorption and the narrow quasi-particle mode which evolves with an extremely small scattering rate at low temperatures.^{12,13} It therefore seems worth to revisit the issue of quasi-particle response in a conventional superconductor. Here we give the first report on the temperature and frequency dependence of the complex conductivity of aluminum in a very wide energy range ($3 \cdot 10^{-4} < \hbar\omega/2\Delta(0) = hf/2\Delta(0) < 0.3$ and $T/T_c > 0.5$); we investigate the dynamics of the quasi-particles and the influence of the mean free path.

II. EXPERIMENT

Aluminum films of different thickness (30 to 50 nm) were thermally evaporated (rate 1 nm/s) onto sapphire substrates. The film thickness was determined by a quartz microbalance, atomic force microscopy, and ellipsometry. In order to vary the mean free path, the films were prepared at different partial pressures of oxygen, as listed in Tab. I. For technical reasons, the films were exposed to air, resulting in an Al_2O_3 layer of approximately

2 nm, before electrical contacts were made by evaporating 100 nm thick gold pads which adapt the geometry of the coaxial connector used for the high-frequency measurements (cf. inset of Fig. 2). The critical temperature T_c was determined from the resistance between the contacts; the width of the superconducting transition is typically 10 mK.

The microwave conductivity was measured with a Corbino spectrometer based on a HP8510C vector network analyzer in the range from 45 MHz to 40 GHz.¹⁴⁾ The data analysis – from complex reflection coefficient via sample impedance to complex conductivity – is done for each frequency separately and requires no additional assumptions except the sample being thin compared to the skin depth δ (which in the complete frequency and temperature range exceeds 10 μm). For cryogenic measurements ($T > 1.1$ K) a full three-standards calibration was performed. Bulk aluminum and a teflon disk were used as short and open end, respectively. NiCr films (25 nm thickness, 80% Ni and 20% Cr) serve as a frequency-independent load ($Z \approx 7 \Omega$). The calibration by the short is most crucial; checks in the normal state of aluminum (where the impedance is frequency independent) and data analysis with different calibrations rule out artifacts. The thin oxide layer between the Al film and the Au contacts acts as a capacitor with a noticeable but correctable effect below 5 GHz; its influence vanishes for higher frequencies. The influence of the oxide layer is temperature independent and the additional impedance can be subtracted from the sample impedance. Fig. 3 demonstrates the effect of the additional capacitor in the superconducting state. While at higher frequency the curves become identical, the corrections are appreciable at low frequencies.

The mean free path ℓ of our films is evaluated from the dc resistivity ρ in the normal state: $\ell = v_F m / (n e^2 \rho)$ with the carrier concentration $n = 6.45 \cdot 10^{22} \text{ cm}^{-3}$ and mass $m = 1.4m_e$ (m_e is the free electron mass).¹⁵ The coherence length is related to the transition temperature: $\xi_0 = 0.18\hbar v_F / (k_B T_c)$, where $v_F = 2.03 \cdot 10^8 \text{ cm/s}$ is the Fermi velocity. The values are listed in Tab. I. Because the samples are in the so-called dirty local limit,^{1,2}

TABLE I: Characteristic parameters of the aluminum films. d is the film thickness, p is the controlled oxygen pressure during evaporation, Z is the sample impedance at $T = 300$ K, ρ is the room temperature resistivity, ℓ refers to the mean free path; the low-temperature skin depth for $f = 40$ GHz is denoted by δ ; T_c is the critical temperature, $\xi(0)$ is the effective coherence length, and $\lambda(0)$ is the effective penetration depth.

	d (nm)	p (μTorr)	Z (Ω)	ρ ($\mu\Omega\text{cm}$)	ℓ (nm)	δ (μm)	T_c (K)	$\xi(0)$ (nm)	$\lambda(0)$ (nm)
A	40	1.2	1.65	32	5.0	15	1.70	61	200
B	30	20	1.25	43	3.7	17	1.75	53	228
C	50	30	2.90	87	1.8	24	1.90	35	310

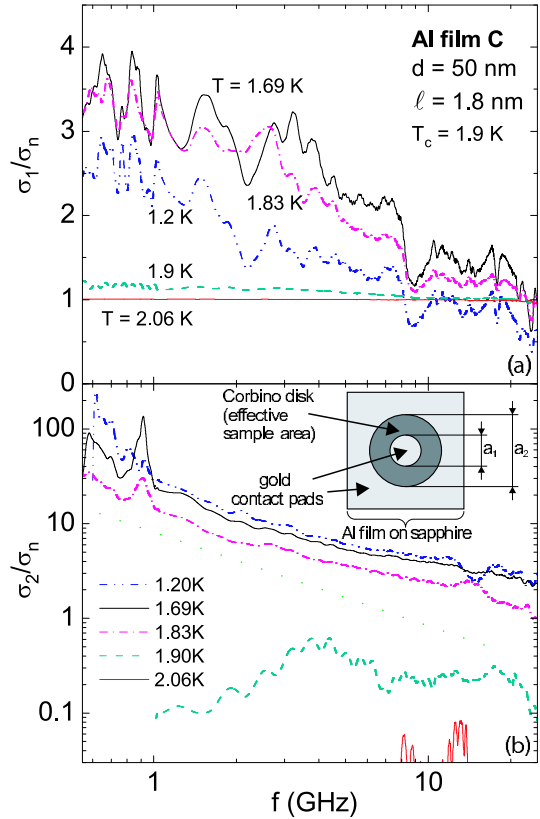


FIG. 2: (color online) Frequency dependence of the complex conductivity of the aluminum film C ($T_c = 1.9$ K), normalized to the metallic conductivity $\sigma_n = \sigma_1(T = 2.1$ K). (a) Real part of the conductivity; note that σ_1 does not vary monotonously with temperature, but goes through a maximum around $T \approx 1.69$ K. (b) The imaginary part is plotted on a double-logarithmic scale in order to demonstrate the $\sigma_2 \propto 1/f$ behavior (green dots). The inset is a sketch of the Corbino arrangement: $a_1 = 0.8$ mm, $a_2 = 1.75$ mm.

both the effective coherence length $\xi(0) = 0.855\sqrt{\xi_0\ell}$ and penetration depth $\lambda(0) = \lambda_L\sqrt{\xi_0/(1.33\ell)}$ are larger than the London penetration depth of bulk aluminum $\lambda_L = 15$ nm. For all films the condition $\ell < \xi(0) < \lambda(0)$ is easily fulfilled. Our results are in good agreement with previous investigations of granular Al films.¹⁶

III. RESULTS

A. Conductivity

The frequency-dependent real and imaginary parts of the normalized conductivity are plotted in Fig. 2 for the film C, as an example. For the metallic state conductivity, we have chosen $\sigma_1(T = 2.1$ K) independent of frequency. σ_1/σ_n increases rapidly as the temperature is reduced below $T_c = 1.9$ K, it goes through a maximum around 1.69 K and then drops again. Theory^{1,2} predicts a $(\sigma_1/\sigma_n)_{\text{max}} \propto \log\{2\Delta(0)/\hbar\omega\}$ frequency behavior of

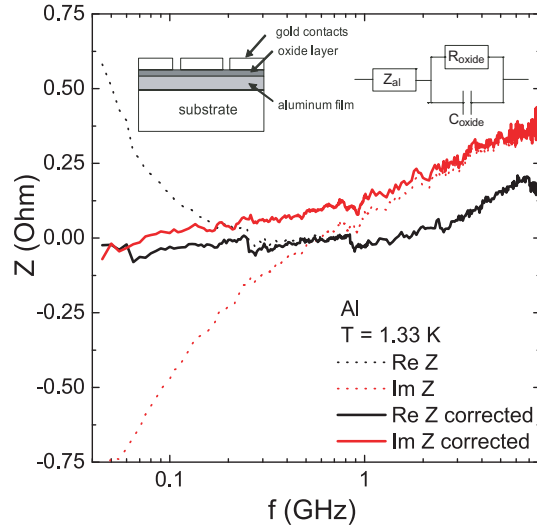


FIG. 3: (color online) Real and imaginary parts of the frequency-dependent impedance Z . The dashed lines indicate the uncorrected impedance of a superconducting aluminum film. The solid lines show the impedance after the correction for the oxide layer between aluminum film and gold contacts. This correction is performed assuming the lumped circuit shown in the inset: Z_{al} is the impedance of the aluminum film under study whereas R_{oxide} and C_{oxide} represent the resistive and capacity contribution of the oxide layer.

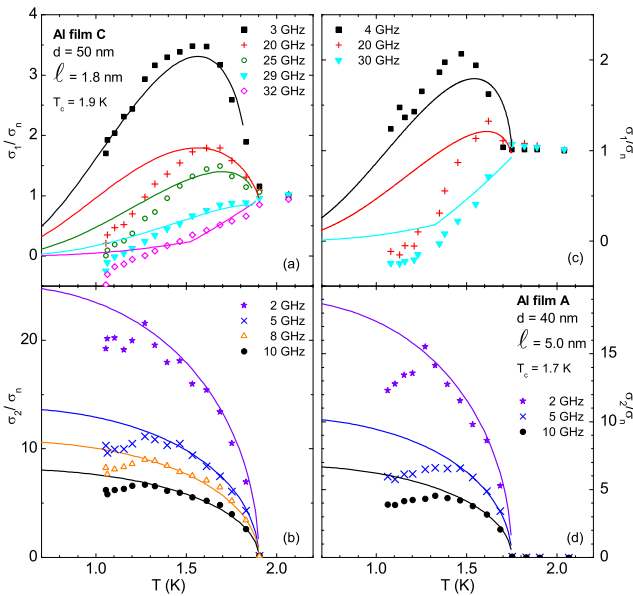


FIG. 4: (color online) Temperature dependence of the (a and c) real and (b and d) imaginary parts of the conductivity of aluminum normalized to the normal state conductivity σ_n . The frames (a) and (b) show the data measured on the Sample C at various frequencies as indicated. The solid lines are calculated by the BCS using $\ell/(\pi\xi) = 0.03$. The frequencies are chosen in a way to demonstrate the effects most clearly. The results of Sample A are displayed in panels (c) and (d). The respective calculations are performed with $\ell/(\pi\xi) = 0.1$.

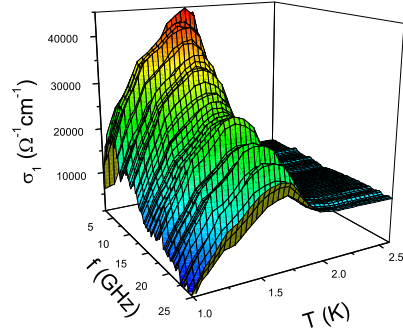


FIG. 5: (color online) Real part of the conductivity of aluminum film C ($T_c = 1.9$ K) as a function of frequency and temperature. The coherence peak decreases in height as the frequency increases. For comparison with Fig. 1, it should be noted that the superconducting energy gap $2\Delta(0) \approx 140$ GHz, which implies that we focus on the very low frequency part [$\hbar\omega/2\Delta(0) < 0.2$].

the maximum, and experimentally we observe this with the roughly linear curve for $T = 1.69$ K in Fig. 2a. An even better description is obtained by a Drude response with a non-monotonous temperature dependence of the spectral weight as will be discussed below (inset of Fig. 9 and Fig. 7).

The imaginary part σ_2 describes the response of the Cooper pairs to the electric field. For small frequencies

$$\frac{\sigma_2(\omega, T)}{\sigma_n} = \frac{\pi\Delta(T)}{\hbar\omega} \tanh \left\{ \frac{\Delta(T)}{2k_B T} \right\} \quad (1)$$

in good agreement with our findings plotted in Fig. 2b, in particular the linear contribution can be seen by comparing with the dotted line in that figure. In Fig. 4b and d, σ_2/σ_n is plotted for various frequencies as a function of temperature. Not too close to T_c , when $\Delta > 2k_B T$, the temperature dependence of σ_2 basically follows the opening of the superconducting gap $\Delta(T)$, according to Eq. (1). For all frequencies, the behavior can be fitted by the BCS prediction, assuming $\ell/(\pi\xi) = 0.1$ for Film A and 0.03 for Film C, in fair agreement with the values calculated in Tab. I.

Figs. 4a and c show data (taken on Sample C and A at different frequencies) of the temperature dependence of the real part of the conductivity. σ_1 is governed by charge carriers thermally excited across the gap; their density of states diverges at the gap edge as depicted in Fig. 6. Right below T_c , $\Delta(T)$ is small: the thermal energy but also the photon energy $\hbar\omega$ are sufficient to break up Cooper pairs. The coherence factor $F(\mathcal{E}, \mathcal{E}')$, which describes the quasi-particle scattering, depends on their energy \mathcal{E} and \mathcal{E}' . If summed over all \mathbf{k} values, it reads¹ $F(\Delta, \mathcal{E}, \mathcal{E}') = \frac{1}{2} (1 + \Delta^2/\mathcal{E}\mathcal{E}')$; only for energies close to the gap Δ , this factor is appreciable: $F \approx 1$. Hence the coherence peak is seen as a maximum in $\sigma_1(T)$ at approximately $0.8 T_c$ in the low-frequency

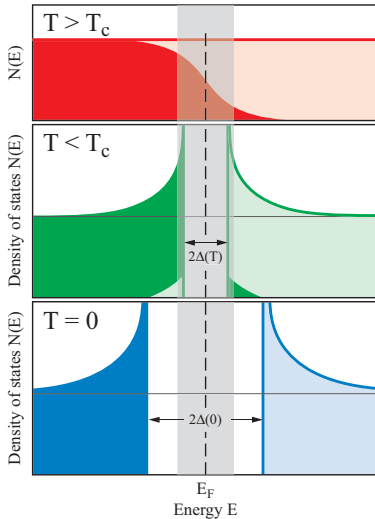


FIG. 6: (color online) Density of electronic states around the Fermi energy E_F . In the normal state ($T > T_c$), the density of states is basically constant; the states are occupied according to the Fermi distribution (dark filled area). For $T < T_c$ the gap opens, and the density of states exhibits a singularity. At finite temperatures there are still states occupied above E_F and state empty below; these are the ones which contribute to the quasi-particle conductivity. For $T = 0$ the gap is complete and no quasi-particle excitations are possible up to $\hbar\omega = 2\Delta(0)$. The grey-shaded area depicts the range which corresponds to the finite energy $\hbar\omega$ of our microwave radiation. It can be considered as a smearing of the border between occupied and empty states similar to the thermal broadening.

limit; it becomes smaller with increasing frequency and shifts to higher temperatures; this is clearly observed in Fig. 4. Above 28 GHz [corresponding to $0.2 \cdot \Delta(0)$] the peak is completely suppressed, and for higher frequencies $\sigma_1(T)$ monotonously drops below T_c . Our findings of the frequency- and temperature-dependent conductivity of Al are summarized in the three-dimensional representation of Fig. 5; we can follow the evolution of the coherence peak over a substantial part of the temperature-frequency space.

B. Spectral Weight

Based on general electrodynamics,² the spectral weight

$$I = \int \sigma_1(\omega) d\omega = \frac{\pi n e^2}{2m} \quad (2)$$

is a measure of the charge carrier density n . In Fig. 7 we plot the spectral weight I^s for the superconducting state by integrating the experimental data of σ_1 between 1 and 40 GHz.¹⁷ We see that the effective carrier concentration increases below the transition temperature, passes through a maximum around 1.6 K and vanishes for $T \rightarrow 0$ in an exponential fashion. This behavior is

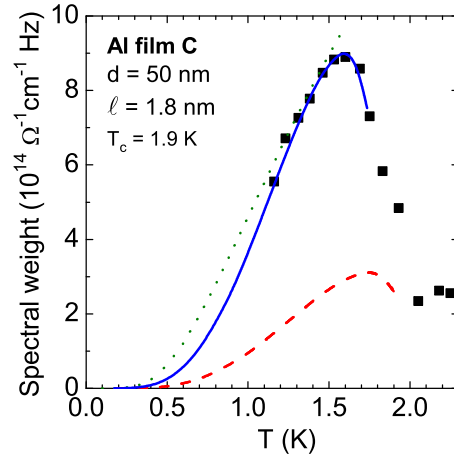


FIG. 7: (color online) Temperature dependence of the spectral weight $I^s(T)$ for the Sample C (squares) evaluated according to Eq. (2). The dashed red line represents the spectral weight obtained by integrating the conductivity calculated by the BCS model (cf. Fig. 8) up to 40 GHz. If we scale the theoretical curve in temperature and spectral weight to the maximum of the data (shown by the solid blue line), the description of the experimental values is excellent. The increase below T_c is due to the enhanced density of states as the superconducting gap opens. After a maximum is reached around 1.6 K, the spectral weight collapses because fewer quasi-particles can be excited across the gap when $T \rightarrow 0$. The low-temperature behavior can be approximated by an exponential law (dotted green line).

perfectly explained by the BCS theory (dashed and full curve in Fig. 7). Here Fig. 6 may serve as an illustration: As the temperature drops below T_c the superconducting gap opens gradually. Due to the finite temperature T , there are still states occupied above the gap and empty states below. These are subject to single particle excitation at arbitrarily small energies, which leads to the quasi-particle contribution in the optical conductivity. The divergence in the density of states causes the increase of that part of spectral weight. Of course, there is a second contribution to $I^s(T)$ given by the electrons excited across the superconducting gap $2\Delta(T)$ (but not accessed in our experiment).

The corresponding conductivity is plotted in Fig. 8. The calculations are done according to the BCS model,⁶ using the formulas of Mattis and Bardeen.⁴ To closely simulate the behavior of aluminum, we assume a transition temperature $T_c = 1.9$ K; the superconducting energy gap is given by $2\Delta(0)/h = 140$ GHz. As the temperature drops slightly below T_c , a narrow zero-frequency mode builds up which grows continuously until it reaches a maximum around $T = 1.6$ K. As the temperature is reduced further, two effects cause the spectral weight (as summed over the experimentally accessible frequency range, the shaded region in Fig. 8) of the single-particles to decrease: the energy gap becomes larger and the Fermi distribution sharpens. Consequently, the number

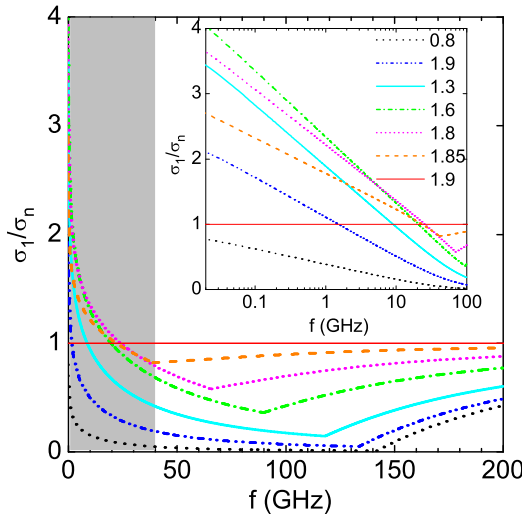


FIG. 8: (color online) Frequency-dependent conductivity of aluminum at different temperatures calculated according to the BCS theory,⁶ formulated by Mattis and Bardeen.⁴ For the critical temperature we assumed $T_c = 1.9$ K, the superconducting energy gap $2\Delta(0)/h = 140$ GHz. The inset, with the clear correspondence to our experimental data in Fig. 2a, illustrates the rapid growth of the zero-frequency quasi-particle peak as the temperature drops below T_c ; for $T < 1.6$ K it becomes narrower and eventually vanishes as $T \rightarrow 0$. The frequency range covered by our experiments is indicated by the grey-shaded area.

of quasi-particles available for transport, and accordingly $I^s(T)$, decreases and finally vanishes for $T \rightarrow 0$. As demonstrated in Fig. 7 the theoretical curve (solid line) nicely describes the experimental findings (squares).

We can describe the drop of spectral weight by the exponential freezing out of the normal carriers; as demonstrated by the dotted line in Fig. 7. Since the total spectral weight has to be conserved² this drop has to be recovered. The Tinkham-Glover-Ferrell sum rule^{18,19} states that the spectral weight

$$A = I^n - I^s = \int_{+0}^{\infty} [\sigma_1^n - \sigma_1^s] d\omega \quad (3)$$

missing in the superconducting state below the gap is transferred to the δ -peak at $\omega = 0$.

C. Scattering Rate

By now we have assumed that the real part of the conductivity is solely determined by the density of states and coherence factor; i.e. the quasi-particle concentration n increases and eventually vanishes according to the temperature dependence of the spectral weight $I(T)$ defined in Eq. (2): $n(T) = (2/\pi)I(T)m/e^2$. Also the spectral behavior of the conductivity $\sigma_1(\omega)$ is given by the density of states $N(E)$. In the course of exploring the microwave properties of high-temperature superconductors,

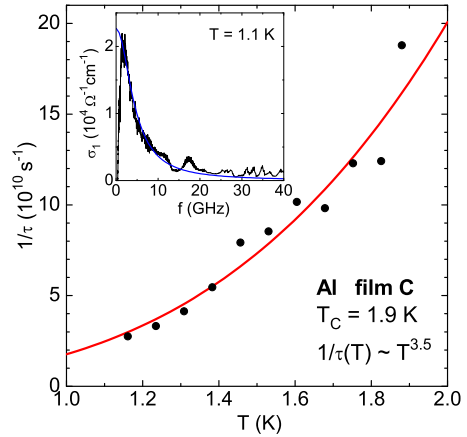


FIG. 9: The temperature-dependent scattering rate for the aluminum Film C. The solid line corresponds to a fit $1/\tau = A + B \cdot T^\alpha$ with $A = 0$, $B = (17.6 \pm 3.3) \cdot 10^{10}$ and $\alpha = 3.5 \pm 0.3$. The inset shows an example of a conductivity spectrum ($T = 1.116$ K) fitted by the Drude model Eq. (4).

a debate arose whether information on the quasi-particle scattering can be obtained.^{20,21,22} In fact, we can fit the real part of the optical conductivity $\sigma_1(\omega)$ by the Drude formula²

$$\sigma_1(\omega) = \frac{ne^2\tau}{m} \frac{1}{1 + (\omega\tau)^2} \quad (4)$$

quite well at least for the lowest temperatures (inset of Fig. 9) and may extract a width which is related to the scattering rate $1/\tau$ within this model. The results for Film C are plotted in Fig. 9 for different temperatures. The temperature-dependent scattering rate can be fitted by a power-law $1/\tau(T) \propto T^\alpha$ with the power $\alpha = 3.5 \pm 0.3$. Similar observations for the case of niobium have been reported previously.^{10,21} It should be pointed out, however, that this approach assumes a constant density of states, which might change with temperature according to the two-fluid model or similar models, but exhibits no energy dependence in the vicinity of the Fermi energy E_F .

D. Influence of the Mean Free Path

In order to get more information on the scattering effects, we prepared films with different defect concentration. The mean free path of the normal state carriers strongly influences the superconducting behavior and the dynamics of the quasi-particles. Accordingly the complex conductivity appreciably varies for samples with different ℓ . Let $\sigma^* = (\sigma_1)_{\text{max}}$ be the maximum of the coherence peak and T^* the width, defined as the temperature difference $T^* = T_c - T_n$ for which $\sigma_1(T = T_n) = \sigma_n$ again. In Fig. 10a the peak width is plotted as a function of mean free path as obtained from Al films grown with different oxygen pressure. Since also the critical tem-

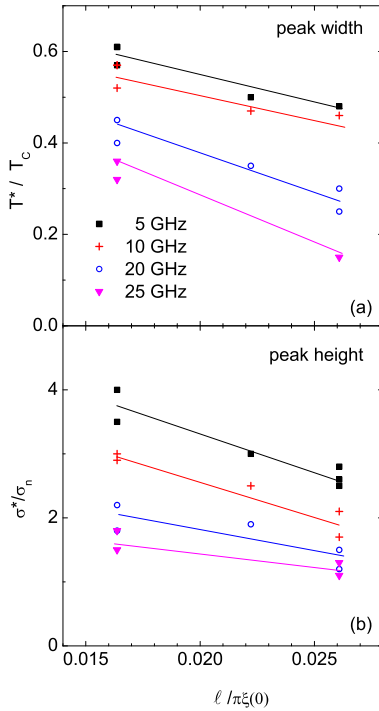


FIG. 10: (color online) (a) Width $(T_c - T_n)/T_c$ and (b) height $(\sigma_1^*)_{\max}/\sigma_n$ of the conductivity coherence peak for aluminum films with different mean free path ℓ , normalized to the effective coherence length $\xi(0)$. The data are taken at various frequencies from 5 to 25 GHz; the lines correspond to a linear interpolation. The multiple data points indicate independent measurements of different samples.

perature T_c and the energy gap Δ depend on the thickness and quality of the films (Tab. I), ℓ is normalized to the effective coherence length. The width of the coherence peak T^* is a measure of how fast the energy gap opens. But it also tells how significant the coherence factor F is in the scattering process: with increasing $\ell/(\pi\xi)$ the finite-frequency conductivity $\sigma_1(\omega)$ decreases more rapidly. The height of the coherence peak σ^*/σ_n is displayed in Fig. 10b, for the different films. When $\ell/(\pi\xi)$ gets larger, σ^* decreases; or with other words, with increasing sample quality the coherence peak be-

comes smaller. The effect is more dramatic for lower frequencies. The ratio of mean free path and coherence length basically indicates whether the scattering takes place within the range in which the phase coherence of the superconducting wavefunction is observed; only then coherence effects matter. Eventually we approach the clean-limit superconductor, for which changes in the ac conductivity below T_c become increasingly difficult to detect.¹³ In a clean-limit superconductor, less spectral weight is transferred from the gap region to the δ -peak.¹ According to $\lambda = c/\sqrt{8A}$, the reduced spectral weight of the δ -peak is in agreement with an increase of the penetration depth, as listed in Tab. I.

IV. CONCLUSIONS AND OUTLOOK

In conclusion, by performing high-precision microwave experiments in a large spectral range down to low temperatures, we were able to map the frequency and temperature dependence of the conductivity coherence peak of aluminum with intentionally reduced mean free path. The influence of the quasi-particle scattering summarized in the coherence effects are elucidated by varying the mean free path of the carriers. For large ℓ , aluminum approaches a clean-limit superconductor and the coherence peak vanishes. The Tinkham-Glover-Ferrell sum rule is obeyed. Our experiments provide a unique possibility to investigate within one material system how scattering and the variation of the mean free path influences the superconducting properties.

Our experiments show that microwave spectroscopy allows for a detailed observation of coherence and scattering properties in superconductors. While our present work focussed on the well-known, conventional superconductor aluminum, future studies can be devoted to unconventional superconductors.

V. ACKNOWLEDGMENTS

We thank M. Dumm, J. Pflaum, and E. Ritz for help and discussions. The theoretical curves were created by the FORTRAN program of E.H. Brandt (Stuttgart). The work was supported by the DFG.

¹ M. Tinkham, *Introduction to Superconductivity*, 2nd edition, (Mc Graw-Hill, New York, 1996).

² M. Dressel and G. Grüner, *Electrodynamics of Solids* (Cambridge University Press, Cambridge, 2002).

³ J. Bardeen, L.N. Cooper, and J.R. Schrieffer, Phys. Rev. **108**, 1175 (1957).

⁴ D. Mattis and J. Bardeen, Phys. Rev. **111**, 412 (1958).

⁵ R.E. Glover and M. Tinkham, Phys. Rev. **108**, 243 (1957); D.M. Ginsberg, P.L. Richards, and M. Tinkham, Phys. Rev. Lett. **3**, 337 (1959); M.A. Biondi and M.P. Garfunkel, Phys. Rev. **116**, 853 (1959); D.M. Ginsberg and M. Tinkham, Phys. Rev. **118**, 990 (1960); P.L. Richards and M.

Tinkham, Phys. Rev. **119**, 575 (1960); L.H. Palmer and M. Tinkham, Phys. Rev. **165**, 588 (1968).

⁶ W. Zimmermann, E.H. Brandt, M. Bauer, E. Seider, and L. Genzel, Physica C **183**, 99 (1991).

⁷ L.C. Hebel and C.P. Slichter, Phys. Rev. **107**, 901 (1957); Phys. Rev. **113**, 1504 (1959).

⁸ J. R. Waldrum, Adv. Phys. **13**, 1 (1964).

⁹ K. Holczer, O. Klein and G. Grüner, Solid State Commun. **78**, 875 (1991)

¹⁰ O. Klein, E.J. Nicol, K. Holczer, and G. Grüner, Phys. Rev. B **50** 6307 (1994).

¹¹ D.N. Basov and T. Timusk, Rev. Mod. Phys. **77**, 721

(2005).

¹² A. Pimenov, A. Loidl, G. Jakob, and H. Adrian, Phys. Rev. B **59**, 4390 (1999).

¹³ P.J. Turner, R. Harris, S. Kamal, M.E. Hayden, D.M. Broun, D.C. Morgan, A. Hosseini, P. Dosanjh, G.K. Mullins, J.S. Preston, R. Liang, D.A. Bonn, and W. N. Hardy, Phys. Rev. Lett. **90**, 237005 (2003).

¹⁴ M. Scheffler and M. Dressel, Rev. Sci. Instrum. **76**, 074702 (2005); M. Scheffler, S. Kilic, and M. Dressel, Rev. Sci. Instrum. **78**, 086106 (2007); E. Ritz and M. Dressel, J. Appl. Phys. **103**, 084902 (2008).

¹⁵ N.W. Ashcroft and N.D. Mermin, *Solid State Physics* (Saunders College Publishing, Philadelphia, 1976)

¹⁶ R.W. Cohen and B. Abeles, Phys. Rev. **168**, 444 (1968).

¹⁷ Extrapolating the data to zero-frequency and expanding the integration below 1 GHz does not change the findings qualitatively. The error in absolute value remains below 5%. As depicted in Fig. 1, the upper cutoff frequency falls right in the range where the quasi-particle contribution to the optical conductivity is already considerably reduced: $\sigma_1^s < \sigma_1^n$.

¹⁸ R.E. Glover and M. Tinkham, Phys. Rev. **104**, 844 (1956); Phys. Rev. **108**, 243 (1957).

¹⁹ R.A. Ferrell and R.E. Glover, Phys. Rev. **109**, 1398 (1958).

²⁰ D.A. Bonn, P. Dosanjh, R. Liang, and W.N. Hardy, Phys. Rev. Lett. **68**, 2390 (1992); A. Hosseini, R. Harris, S. Kamal, P. Dosanjh, J. Preston, R. Liang, W.N. Hardy, and D.A. Bonn, Phys. Rev. B **60**, 1349 (1999).

²¹ O. Klein, Phys. Rev. Lett. **72**, 1390 (1994).

²² D.A. Bonn, K. Zhang, S. Kamal, R. Liang, P. Dosanjh, W.N. Hardy, C. Kallin, and A.J. Berlinsky, Phys. Rev. Lett. **72**, 1391 (1994).